Cross influences of ozone and sulfate precursor emissions changes on air quality and climate

Nadine Unger*†, Drew T. Shindell*, Dorothy M. Koch*, and David G. Streets‡

*NASA Goddard Institute for Space Studies and Columbia University, New York, NY 10025; and ‡Argonne National Laboratory, Argonne, IL 60439

Edited by Jack Halpern, University of Chicago, Chicago, IL, and approved January 30, 2006 (received for review October 6, 2005)

Tropospheric O_3 and sulfate both contribute to air pollution and climate forcing. There is a growing realization that air quality and climate change issues are strongly connected. To date, the importance of the coupling between O_3 and sulfate has not been fully appreciated, and thus regulations treat each pollutant separately. We show that emissions of O_3 precursors can dramatically affect regional sulfate air quality and climate forcing. At 2030 in an A1B future, increased O_3 precursor emissions enhance surface sulfate over India and China by up to 20% because of increased levels of OH and gas-phase SO_2 oxidation rates and add up to 20% to the direct sulfate forcing for that region relative to the present day. Hence, O_3 precursors impose an indirect forcing via sulfate, which is more than twice the direct O_3 forcing itself (compare −0.61 vs. +0.35 W/m²). Regulatory policy should consider both air quality and climate and should address O_3 and sulfate simultaneously because of the strong interaction between these species.

air pollution | climate change | aerosols | greenhouse gases

The interconnectedness between air quality and climate change issues through non-CO_2 greenhouse gases and aerosols is of emerging interest (1–5). Ozone (O_3) and sulfate, both radiatively active air pollutants, are key players in that interconnection. Moreover, O_3 and sulfate are themselves strongly coupled through tropospheric photochemistry and emission source types (primarily fossil-fuel burning). Several interactive global models of tropospheric O_3 and sulfate have been developed (6–9). However, the influence of the O_3–sulfate interaction on climate has not yet been isolated and quantified.

Both O_3 and sulfate are secondary pollutants, formed during the photo-oxidation of directly emitted precursor species. Sulfate aerosol is formed from the oxidation of sulfur dioxide (SO_2), and O_3 is formed during the oxidation of carbon monoxide (CO), methane (CH_4), or nonmethane volatile organic compounds (NMVOCs) in the presence of nitrogen oxides (NO_x). SO_2 has two main oxidation pathways: in the gas phase by the hydroxyl radical (OH) or in the aqueous phase (for example, inside cloud droplets) by hydrogen peroxide (H_2O_2) or O_3 (globally, the H_2O_2 reaction is of much more importance than the O_3 reaction). O_3 is the source gas for OH and hence, indirectly, H_2O_2, which is formed under low NO_x conditions as a chain termination product of the catalytic photochemical cycling that produces O_3. The gas-phase SO_2 oxidation pathway leads to the formation of new particles in the atmosphere. The aqueous-phase sulfate formation is typically a faster process than the gas-phase OH-initiated oxidation, and on regional and global scales, more sulfate is generated through the aqueous pathway. However, the lifetime of the sulfate generated in the aqueous phase is shorter than in the gas phase because the sulfate near or within a cloud is prone to scavenging if the cloud precipitates (10). Hence, the environmental consequences of the man-made SO_2 emissions through sulfate formation, be they acid rain, direct or indirect climate forcing, or air pollution, are dependent somewhat on the oxidation pathway. Sulfate aerosol feeds back on O_3 and the oxidant chemistry by providing a surface for the conversion of NO_x to nitric acid, a highly soluble and easily removable species, thus limiting the rate of O_3 formation.

In the near future, man-made emissions of the precursor gases (CO, CH_4, NMVOCs, NO_x, and SO_2) will change and influence the distributions of sulfate and O_3 in the troposphere. Changes in physical climate also will influence the sulfate and O_3 distributions and lifetimes. For example, changes in the hydrological cycle would impact the wet deposition rates of sulfate aerosol and O_3 precursor species. In addition to the direct influence of changes in the precursor gases for each species, interactions between the O_3 and sulfate cycles also will change because of the altered precursor emissions and climate. Changes in the tropospheric oxidants (OH, H_2O_2, and O_3) driven either by changes in O_3 precursor gases or climate, will influence sulfate formation. Conversely, changes in sulfate will affect O_3 through altering the heterogeneous conversion of NO_x to HNO_3.

The impacts of man-made emissions and physical climate changes on O_3 and sulfate tropospheric composition at 2030 recently were examined for a broad range of possible futures (11). A commonality across future man-made emissions projections is a regional shift with decreases at NH midlatitudes and increases at the more photochemically active subtropical and tropical latitudes. In the Intergovernmental Panel on Climate Change A1B future, the man-made emissions changes dominated the impacts of physical climate changes on sulfate and O_3 composition. Hence, we select that scenario for further sensitivity analyses of the future O_3 and sulfate coupling. We quantify the influence of changes in oxidants (driven by changes in man-made O_3 precursor emissions) on sulfate aerosol and changes in sulfate aerosol (driven by changes in man-made SO_2 emissions) on O_3. A similar study that investigated the impacts of man-made emissions changes between 1985 and 1996 on the SO_2 budget and oxidant concentrations has been carried out (9). They found that increases in SO_2 emissions over China caused a dampening of the O_3 increase by 4 parts per billion by volume (ppbv) at 955 hPa because of sulfate formation, but they did not quantify radiative impacts of the sulfate and O_3 changes.

We apply the Goddard Institute for Space Studies (GISS) Atmospheric Composition-Climate Model to investigate future interactions between tropospheric O_3 and sulfate aerosol. Further details of the model system and the emissions scenarios may be found in *Methods*. The simulations set is described in Table 1. The 2030 control simulation (2030C) uses future 2030 projections of both O_3 and sulfate precursor emissions. Two additional sensitivity simulations are performed ($2030SO_4$ and $2030O_3$). In $2030SO_4$, the man-made SO_2 emissions change according to the 2030 A1B scenario, while the man-made O_3 precursor emissions (NO_x, CO, and NMVOCs) and CH_4 concentrations are held to values from the 1995 present-day control simulation. The $2030O_3$ includes future 2030 projections of

Conflict of interest statement: No conflicts declared.

This paper was submitted directly (Track II) to the PNAS office.

Freely available online through the PNAS open access option.

Abbreviations: GISS, Goddard Institute for Space Studies; NMVOC, nonmethane volatile organic compound; NO_x, nitrogen oxides; 2030C, 2030 control simulation.

†To whom correspondence should be addressed. E-mail: nunger@giss.nasa.gov.

Table 1. Description of simulations

Simulation name	Sulfate precursor emissions year (SO_2)	O_3 precursor emissions year (CO, NO_x, NMVOCs)	Climatic boundary conditions (sea surface temperatures and sea ice)	CH_4 concentration, ppbv	
				NH	SH
1995C	1995	1995	1990s	1802	1655
2030C	2030	2030	2030s	2603	2353
$2030SO_4$	2030	1995	2030s	1802	1655
$2030O_3$	1995	2030	2030s	2603	2353

ppbv, parts per billion by volume.

man-made NO_x, CO, and NMVOCs emissions and CH_4 concentrations, but man-made SO_2 emissions are held to present-day 1995 values.

Results

Surface Air Quality. We compare simulations $2030SO_4$ and 2030C to assess the role of future emissions-driven changes in oxidants on sulfate aerosol. Fig. 1 shows the percentage difference in surface sulfate mixing ratio between 2030C and $2030SO_4$ [i.e., $100 \times (2030C - 2030SO_4)/2030C$]. Surface sulfate mixing ratios are increased by >10% over much of South Asia, the Middle East, North Africa, and the most developed parts of South America because of the increases in O_3 precursor emissions alone. The largest influence occurs over the Indian subcontinent, where the surface sulfate is 20% greater as a result of the future emissions-driven increases in oxidants.

Comparing simulations $2030O_3$ and 2030C to assess the role of future emissions-driven changes in sulfate aerosol on surface O_3, we found negligible (<1%) changes in surface O_3 at NH midlatitudes (data not shown), indicating that the future reductions in SO_2 emissions in those regions have a very small impact on surface O_3. The largest influence occurs around the tropical latitude belt with O_3 differences of only approximately +1 parts per billion by volume for the simulation with present-day SO_2 emissions but future O_3 precursor emissions relative to the full 2030 simulation.

Sulfate Budget and Oxidation Pathways. The tropospheric sulfate budget for four different tropospheric regions in the 2030C and $2030SO_4$ simulations are presented in Table 2. The regions are not strict geopolitical definitions and have different spatial sizes. The regional budgets do not balance because of transport into and out of the individual regions. Over India and China, when the O_3 precursor emissions are held at present-day values in the 2030 A1B future, the gas-phase oxidation of SO_2 is reduced (≈20%) and the aqueous-phase oxidation is increased (5%) relative to the control run. These results imply that the increased O_3 precursor emissions at 2030 over India and China drive greater gas-phase oxidation, which is only partially compensated for by a reduction in aqueous-phase oxidation. This effect is most likely a result of the NO_x emissions increases causing a shift to a high NO_x chemistry regime, maintaining significant OH concentrations through recycling and reducing H_2O_2 formation and availability. Over the United States, the opposite effect is seen, and the future reduction in O_3 precursor emissions results in less gas-phase SO_2 oxidation (≈8%). Across Europe there are only minimal differences in the sulfate budget between the 2030C control simulation and $2030SO_4$ in which O_3 precursor emissions

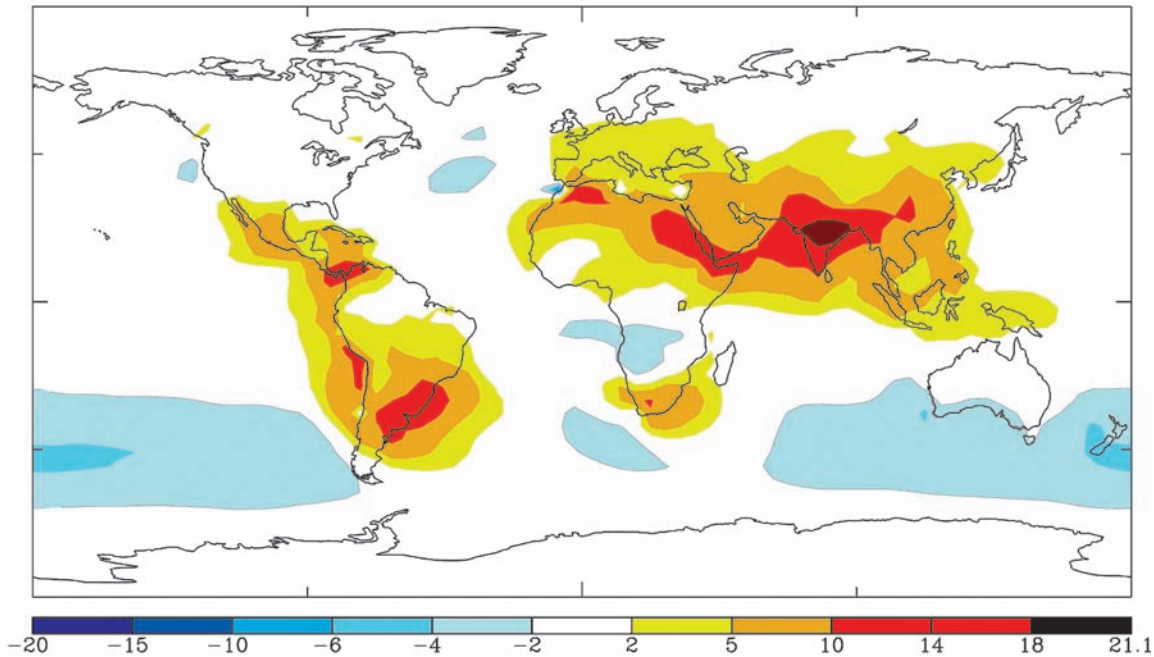

Fig. 1. Percentage difference in surface sulfate mixing ratio between future control simulation (2030C) and sensitivity simulation with future SO_2 emissions but present-day O_3 precursor emissions ($2030SO_4$) [i.e., $100 \times (2030C - 2030SO_4)/2030C$].

Table 2. Tropospheric sulfur budget for four different tropospheric regions for the 2030 A1B future (2030C) and a sensitivity study with O_3 precursor emissions (NO_x, CO, and NMVOCs) and CH_4 concentrations held to present-day values ($2030SO_4$)

Budget term	Simulation	Global	Europe	U.S.	India	China
SO_2 anthropogenic emissions, Tg·S·yr^{-1}	2030	96.0	8.94	2.67	9.74	30.71
Sulfate sources, Tg·S·yr^{-1}						
Gas-phase SO_2 oxidation	2030C	19.6	1.15	0.48	2.15	3.29
	$2030SO_4$	18.4	1.13	0.52	1.78	2.72
In-cloud SO_2 oxidation	2030C	20.0	0.63	0.66	1.88	2.70
	$2030SO_4$	20.0	0.63	0.64	1.97	2.80
Sulfate sinks, Tg·S·yr^{-1}						
Wet deposition	2030C	36.8	1.38	1.34	3.14	5.14
	$2030SO_4$	35.8	1.35	1.34	3.06	4.85
Dry deposition	2030C	5.6	0.28	0.20	0.59	0.87
	$2030SO_4$	5.3	0.27	0.20	0.51	0.79
Burden, Gg·S	2030C	686.3	36.2	36.6	44.1	62.0
	$2030SO_4$	676.7	36.3	37.4	40.8	58.0
Lifetime, days	2030C	5.89	7.97	8.68	4.32	3.77
	$2030SO_4$	6.01	8.18	8.87	4.17	3.76

are held to present-day values. On a global scale, the O_3 precursor emissions changes at 2030 drive an ≈5% increase in gas-phase SO_2 oxidation.

Radiative Forcings. The annual average direct radiative forcings of sulfate and O_3 for the control and sensitivity experiments are presented in Table 3. The difference in global mean sulfate radiative forcing between $2030SO_4$ and 2030C is small (0.02 W/m^2), consistent with the small influence on global sulfate burden (Table 2). However, the regional differences may be much larger. Over India and China the sulfate direct forcing is more positive by up to +0.6 W/m^2 (≈20%) when O_3 precursors remain at present-day values. The impact of the increasing O_3 precursors on the sulfate forcing is almost twice the direct forcing of the O_3 change alone for the India and China regions (compare −0.61 vs. 0.35 W/m^2). A corollary is that reduction of O_3 precursors in Asia would improve both O_3 and sulfate surface air quality but would impose an additional positive forcing on the region through a concomitant reduction in sulfate. The achievement of overall air quality and climate benefits from sulfate and O_3 reductions is complicated by the chemical interdependence of these species.

The difference in global mean O_3 radiative forcing between $2030O_3$ and 2030C is small (≈0.01W/m^2). The O_3 forcing over India and China would be greater by only ≈0.02–0.03 W/m^2, if SO_2 emissions remained at present-day values.

Discussion

Our results indicate that emissions-driven changes in oxidants have a significant effect on sulfate over Asia at 2030 in an A1B future. The increased O_3 precursor emissions contribute 20% of the surface sulfate pollution and 20% of the direct sulfate forcing for that region. The increased O_3 precursors drive greater gas-phase oxidation of SO_2, implying the formation of new particles. Meanwhile, the SO_2 emissions changes do not significantly affect future O_3 through heterogeneous NO_x conversion on sulfate. Air quality or climate-related policy concerning SO_2 emissions must be developed within the context of the changing O_3 precursor emissions and SO_2 oxidation pathways.

Table 3. Annual average sulfate and O_3 direct radiative forcings (W/m^2) for control and sensitivity experiments

Species	Experiment forcing	Global	India and China
Sulfate	2030C–1995C	−0.22	−3.03
	$2030SO_4$–1995C	−0.20	−2.42
O_3	2030C–1995C	+0.14	+0.35
	$2030O_3$–1995C	+0.15	+0.38

For Asia in the near future, the net effect of the change in O_3 precursors on climate is negative, including the indirect sulfate impact, but leads to large increases in both O_3 and sulfate surface air pollution. In our model the annual average surface sulfate mixing ratio over the Indian subcontinent region increases from ≈400 parts per trillion by volume (pptv) in the present day to ≈2,000 pptv in the A1B 2030 future with ≈300–400 pptv of the increase driven entirely by the concomitant changes in O_3 precursor emissions. The annual average surface-level O_3 increases from ≈35 to 60 parts per billion by volume. The potential consequences of such large increases in the sulfate aerosol and O_3 pollution may have devastating social and economic impacts across the Indian subcontinent. There is already substantial evidence that sulfate aerosol and O_3 pose serious public health problems with known adverse impacts on human pulmonary and cardiovascular health (12–16). The increase in sulfate aerosol loading also would be likely to impact the hydrological cycle and climate of the region (17, 18). In addition, both the sulfate aerosol and O_3 increases would have detrimental impacts on plants and ecosystems affecting agriculture and crops through various mechanisms including acidification of soils in the case of sulfate (19, 20).

Methods

Model Description. The GISS Atmospheric Composition-Climate Model system is composed of the new, state-of-the-art GISS ModelE (also called Model III) general circulation model (GCM) (21) with fully interactive chemistry and aerosols (including sulfate, mineral dust, black and organic carbon, and sea salt) that runs seamlessly from the surface up through the lower mesosphere. The model has been designed with a flexibility to switch on all or different combinations of components of the composition to facilitate investigation of individual or collective interactions between the components. The model system is able to capture not only the magnitude and spatial distributions of important trace gases in the atmosphere but also of surface deposition fluxes and reproduces observations (North American, European, and Asian) with a realism comparable with other state-of-the-art composition models worldwide in this regard (22). ModelE offers flexible vertical and horizontal resolution

options. In the present study, we used 23 vertical layers (model top in the mesosphere) and $4 \times 5°$ horizontal resolution.

For the purpose of the present study, we ran with the tropospheric chemistry module fully coupled to the sulfate aerosol module, switching off other aerosol types (23). The tropospheric chemistry module includes the chemistry of HO_x–NO_x–O_x–CO–CH_4, hydrocarbon families, and peroxyacetylnitrates (24). The updated ModelE sulfate aerosol module includes prognostic simulations of the mass distributions of dimethyl sulfide (DMS), methanesulfonic acid (MSA), SO_2, and sulfate (25). In the coupled model configuration, the chemistry and sulfate modules are explicitly linked such that instantaneous concentrations of OH, NO_3, and H_2O_2 are available to the sulfate module and instantaneous concentrations of SO_4, SO_2, and DMS are available to the chemistry module. At present, the sulfate module does not include in-cloud oxidation of SO_2 by O_3.

The CH_4 concentration values used in the study were generated in previous simulations with the same model by using a full CH_4 cycle including climate-sensitive emissions from wetlands (11). For the present-day and future simulations, the climate was specified by prescribed seasonally varying decadal average sea surface temperatures and sea ice that were generated in a previous simulation of the GISS Atmosphere-Ocean Model (26).

Emissions. The present-day anthropogenic trace gas emissions inventory was taken from the Emissions Database for Global Atmospheric Research (EDGAR3.2) representative of the year 1995 (27). The future 2030 trace gas emissions inventory was based on the A1B scenario from the Intergovernmental Panel on Climate Change storyline, which envisages rapid economic growth with a balance between fossil fuel intensive and renewable energy sources. A1B projects significant global increases in all trace gas emissions at 2030. Global anthropogenic emissions of CO, NO_x, NMVOCs, CH_4, and SO_2 increase by 25%, 80%, 65%, 76%, and 33%, respectively, by 2030. Over the U.S. and Western Europe, SO_2 and NO_x emissions decline by up to −80% and −30%, respectively. There are large increases in precursor emissions that occur over India: a 400% increase in SO_2 emissions and a 500% increase in fossil fuel NO_x emissions. Over China, SO_2 emissions increase by ≈30%, and NO_x emissions increase by 100%.

We thank the National Aeronautics and Space Administration (NASA) Center for Computational Sciences for computing support. This work was supported by the NASA Atmospheric Chemistry Modeling and Analysis Program (ACMAP).

1. Hansen, J., Sato, M., Ruedy, R., Lacis, A. & Oinas, V. (2000) *Proc. Natl. Acad. Sci. USA* **97,** 9875–9880.
2. Hansen, J. E. (2002) *Air Pollution as a Climate Forcing* (Natl. Aeronautics Space Administration GISS, New York).
3. Fiore, A. M., Jacob, D. J., Field, B. D., Streets, D. G., Fernandes, S. D. & Jang, C. (2002) *Geophys. Res. Lett.* **29,** 1919.
4. Hansen, J. & Sato, M. (2004) *Proc. Natl. Acad. Sci. USA* **101,** 16109–16114.
5. Shindell, D. T., Faluvegi, G., Bell, N. & Schmidt, G. A. (2005) *Geophys. Res. Lett.* **32,** L04803.
6. Roelofs, G. J., Lelieveld, J. & Ganzeveld, L. (1998) *Tellus B* **50,** 224–242.
7. Tie, X., Brasseur, G., Emmons, L., Horowitz, L. & Kinnison, D. (2001) *J. Geophys. Res.* **106,** 22931–22964.
8. Liao, H., Seinfeld, J. H., Adams, P. J. & Mickley, L. J. (2004) *J. Geophys. Res.* **109,** D24204.
9. Berglen, T. F., Berntsen, T. K., Isaksen, I. S. A. & Sundet, J. K. (2004) *J. Geophys. Res.* **109,** D19310.
10. Koch, D., Park, J. & Del Genio, A. (2003) *J. Geophys. Res.* **108,** 4781.
11. Unger, N., Shindell, D. T., Koch, D. M., Amann, M., Cofala, J. & Streets, D. G. (2006) *J. Geophys. Res.*, in press.
12. Kinney, P. L. (1999) *Semin. Respir. Crit. Care Med.* **20,** 601–607.
13. Pope, C. A. (2000) *Aerosol Sci. Technol.* **32,** 4–14.
14. Ruidavets, J. B., Cournot, M., Cassadou, S., Giroux, M., Meybeck, M. & Ferrieres, J. (2005) *Circulation* **111,** 563–569.
15. Thurston, G. D., Ito, K., Mar, T., Christensen, W. F., Eatough, D. J., Henry, R. C., Kim, E., Laden, F., Lall, R., Larson, T. V., *et al.* (2005) *Environ. Health Perspect.* **113,** 1768–1774.
16. Cohen, A. J., Anderson, H. R., Ostro, B., Pandey, K. D., Krzyzanowski, M., Kunzli, N., Gutschmidt, K., Pope, A., Romieu, I., Samet, J. M. & Smith, K. (2005) *J. Toxicol. Environ. Health* **68,** 1301–1307.
17. Qian, Y., Leung, L. R., Ghan, S. J. & Giorgi, F. (2003) *Tellus B* **55,** 914–934.
18. Ramanathan, V., Chung, C., Kim, D., Bettge, T., Buja, L., Kiehl, J. T., Washington, W. M., Fu, Q., Sikka, D. R. & Wild, M. (2005) *Proc. Natl. Acad. Sci. USA* **102,** 5326–5333.
19. Emberson, L. D., Ashmore, M. R. & Murray, F., eds. (2003) *Air Pollution Impacts on Crops and Forests: A Global Perspective* (Imperial College Press, London).
20. Agrawal, M. (2005) *Natl. Acad. Sci. Lett. India* **28,** 93–106.
21. Schmidt, G. A., Ruedy, R., Hansen, J. E., Aleinov, I., Bell, N., Bauer, M., Bauer, S., Cairns, B., Canuto, V., Cheng, Y., *et al.* (2006) *J. Climate* **19,** 153–192.
22. Lamarque, J.-F., Kiehl, J. T., Brasseur, G. P., Butler, T., Cameron-Smith, P., Collins, W. D., Collins, W. J., Granier, C., Hauglustaine, D., Hess, P. G., *et al.* (2005) *J. Geophys. Res.* **110,** D19303.
23. Bell, N., Koch, D. & Shindell, D. T. (2005) *J. Geophys. Res.* **110,** D14305.
24. Shindell, D. T., Faluvegi, G. & Bell, N. (2003) *Atmos. Chem. Phys.* **3,** 1675–1702.
25. Koch, D., Schmidt, G. & Field, C. (2006) *J. Geophys. Res.*, in press.
26. Russell, G. L., Miller, J. R., Rind, D., Ruedy, R. A., Schmidt, G. A. & Sheth, S. (2000) *J. Geophys. Res.* **105,** 14891–14898.
27. Olivier, J. G. J. & Berdowski, J. J. M. (2001) in *The Climate System*, eds. Berdowski, J., Guicherit, R. & Heij, B. J. (A. A. Balkema, Brookfield, VT), pp. 33–78.